Hindawi
Journal of Nanomaterials
Volume 2021, Article ID 6040219, 1 page
https://doi.org/10.1155/2021/6040219

Retraction

Retracted: Chemical Bath Deposition of PbS:Hg^{2+} Nanocrystalline Thin Films

Journal of Nanomaterials

Received 16 December 2020; Accepted 16 December 2020; Published 29 January 2021

Journal of Nanomaterials has retracted the article titled "Chemical Bath Deposition of PbS:Hg^{2+} Nanocrystalline Thin Films" [1]. As originally raised on PubPeer [2], the article was found to have concerns with some of the Figures. A summary of the concerns is as follows:

(i) Two figures are the same as those in a previous publication [3], despite different doping agents being described in each article (this article used mercury, while [3] used bismuth). Figure 3 is identical to Figure 6 in [2] and Figure 1a is identical to Figure 2(a) in [3].

(ii) Figures 1a, 1b, and 1c are identical to figures in two previous publications, Figures 2b, 2d, and 2f in [4] and the right-hand panels of Figure 2 in [5]. Nickel is stated as the doping agent for [4, 5], while in [1] it is stated as mercury

The journal and the editorial board are retracting the article due to concerns that the data in this article are not reliable. The authors do not agree to retraction.

References

[1] R. Palomino-Merino, O. Portillo-Moreno, L. A. Chaltel-Lima, R. Gutiérrez Pérez, M. de Icaza-Herrera, and V. M. Castaño, "Chemical Bath Deposition of PbS:Hg^{2+} Nanocrystalline Thin Films," *Journal of Nanomaterials*, vol. 2013, Article ID 507647, 6 pages, 2013.

[2] "Chemical Bath Deposition of PbS:Hg^{2+} Nanocrystalline Thin Films," PubPeer, 2019, https://pubpeer.com/publications/C5D39B944A893F1F1AE8F1F026D839.

[3] R. Gutiérrez Pérez, O. Portillo Moreno, L. Chaltel Lima, M. Chévez Portillo, R. Palomino Merino, and M. Zamora Totozintle, "Optical and structural properties of PbS: Bi^{3+} nanocrystals," *Revista Mexicana de Fisica*, vol. 61, pp. 356–362, 2015.

[4] O. Portillo Moreno, L. A. Chaltel Lima, M. Chávez Portillo et al., "Properties of PbS: Ni^{2+} Nanocrystals in Thin Films by Chemical Bath Deposition," *ISRN Nanotechnology*, vol. 2012, Article ID 546027, 12 pages, 2012.

[5] H. Lima Lima, C. Aguilar Galicia, A. Camacho Yáñez et al., "Ni influence, on growth of chemically deposited PbS films," in *Revista Naturaleza Y Tecnologia*, pp. 4–11, Universidad De Guanajuato, 2013.

Hindawi Publishing Corporation
Journal of Nanomaterials
Volume 2013, Article ID 507647, 6 pages
http://dx.doi.org/10.1155/2013/507647

Research Article

Chemical Bath Deposition of PbS:Hg^{2+} Nanocrystalline Thin Films

R. Palomino-Merino,[1] O. Portillo-Moreno,[2] L. A. Chaltel-Lima,[2] R. Gutiérrez Pérez,[3] M. de Icaza-Herrera,[4] and V. M. Castaño[4]

[1] *Facultad de Ciencias Físico Matemáticas, Posgrado en Física Aplicada, Benemérita Universidad Autónoma de Puebla, Avenida San Claudio y 18 Sur, Colonia San Manuel, Ciudad Universitaria, 72570 Puebla, PUE, Mexico*
[2] *Facultad de Ciencias Químicas, Benemérita Universidad Autónoma de Puebla, P.O. Box 1067, 72001 Puebla, PUE, Mexico*
[3] *Laboratorio de Síntesis de Complejos, Facultad de Ciencias Químicas, Benemérita Universidad Autónoma de Puebla, P.O. Box 1067, 72001 Puebla, PUE, Mexico*
[4] *Centro de Física Aplicada y Tecnología Avanzada, Universidad Nacional Autónoma de México, Boulevard Juriquilla 3001, 76230 Santiago de Querétaro, QRO, Mexico*

Correspondence should be addressed to V. M. Castaño; castano@fata.unam.mx

Received 1 February 2013; Revised 24 April 2013; Accepted 20 May 2013

Academic Editor: Rakesh Joshi

Nanocrystalline PbS thin films were prepared by Chemical Bath Deposition (CBD) at 40 ± 2°C onto glass substrates and their structural and optical properties modified by in-situ doping with Hg. The morphological changes of the layers were analyzed using SEM and the X-rays spectra showing growth on the zinc blende (ZB) face. The grain size determined by using X-rays spectra for undoped samples was found to be ~36 nm, whereas with the doped sample was 32–20 nm. Optical absorption spectra were used to calculate the E_g, showing a shift in the range 1.4–2.4 eV. Raman spectroscopy exhibited an absorption band ~135 cm^{-1} displaying only a PbS ZB structure.

1. Introduction

There is increasing interest into deposition of ternary derivative materials due to their potential for designing and tailoring not only the lattice parameters, but also the forbidden band gap energy E_g, by means of the growth parameters [1, 2]. Accordingly, two techniques have been successfully employed: successive ionic layer and reaction (SILAR) [3] and sol gel methods [4]. However, most of the reported studies have been focused on the deposition of ternary derivatives material on thin films as $Cd_{1-x}Zn_xS$ [5], $Cd_{1-x}SCu_x$ [6], $Hg_xCd_{1-x}S$ [7], and $PbS_{1-x}Ni_x$. It must be pointed out that PbS thin films are promising photovoltaic materials, for their E_g can be adjusted to match the ideal ~1.5 eV required for an efficient solar cell [8]. Also, new physical aspects, dependent on size, have generated an ongoing thrust for new practical applications. PbS nanocrystals with grain-size (GS) dimensions in the range 1–20 nm are of technological interest for advanced optoelectronic applications, showing a stronger quantum confinement effect when the crystallite size matches the dimension of Bohr exciton [9]. In this context, there are two situations: the weak confinement and the strong regime [10]. In the weak regime, the radius of the electron-hole pair causes a blue shift in the absorption spectrum, but the range of motion of the exciton is limited. The confinement effect appears as a shift in the absorption spectra to lower wavelengths, due to change in the E_g, which can be controlled through the modification of the surface functionalization [11, 12]. Several schemes for using nanocrystals in solar cells are under active consideration, including nanocrystals-polymer composites [13, 14], and, in the present work, PbS and Hg^{2+}-doped PbS nanostructured films were prepared by chemical bath (CB), in order to investigate structural and optical properties of undoped and doped PbS films. Semiquantitative measurements of atomic concentration of elements and the micrographs were achieved by Electron

Dispersion Spectroscopy (EDS) utilizing a SEM JEOL JSM-6610LV. The crystalline structure characterization was carried out by X-ray diffraction (XRD) patterns recorded in a Bruker D8 Discover Diffractometer, using the Cu $K_{\alpha 1}$ line. The grain size was determined from the Scherrer's formula. The optical absorption spectra, measured employing a Varian CARY 100 Spectrophotometer, allowed to calculate the forbidden band gap energy (E_g) by using the $(\alpha h\nu)^2$ versus Energy plot, where α is the optical absorption coefficient and $h\nu$ the photon energy. The Raman spectra were determined with a micro-Raman System Lab Ram-Idler apparatus with an excitement line of 632.8 nm.

2. Experimental Procedure

The chemical reactions to grow of PbS films doped with Hg^{2+} were determined by employing the reported cell potential values in basic media. The cell potential and the Gibbs free energy are related through the Nernst equations: $\Delta G^\circ = -n\tau\varepsilon^\circ$, where n is the number of equivalents, τ is the Faraday constant, and ε° is the cell potential. The numerical value ΔG° provides thermodynamic information on the possibility of spontaneous chemical reactions. The formation of the coordination complex $[M(NH_3)_4]^{2+}$ is key to release M^{2+} ions ($M^{2+} = Cd^{2+}$, Pb^{2+}, Zn^{2+}, etc.) and their slow recombination with S^{2-} ions which leads to the spontaneous formation of the MS precipitate in an easily controlled process. The growth of PbS is therefore carried out according to the following steps: (a) by mixing $Pb(CH_3CO_3)_2$, KOH, and NH_4NO_3, to produce the coordination complex, $[Pb(NH_3)_4]^2$ is generated indirectly; (b) The S^{2-} ions are found in the solution and generated by the thiourea decomposition in alkaline solution; (c) the aforementioned steps allow the slow process at the substrate surface to take place predominantly over direct hydrolysis of thiourea in the bulk of the reaction bath as follows [15]:

$$SC(NH_2)_2 + 3OH^- \Longleftrightarrow CO_3^{2-} + H_2S + 3H^+ \quad (1)$$

$$[Pb(NH_3)_4]^{2+} + H_2S + S^{2-} \Longleftrightarrow PbS + 4NH_3 + S + 2H^+ + 2e \quad (2)$$

$$\Delta G^\circ = +362.88\ \text{KJ}$$

$$HPbO^- + H_2O + [Pb(NH_3)_4]^{2+} + H_2S + S^{2-} \Longleftrightarrow PbS + 4NH_3 + S + 2H^+ + Pb + OH^- + Pb^{2+} \quad (3)$$

$$\Delta G^\circ = +799.48\ \text{KJ}$$

$$PbS + 2e + 2H^+ \Longleftrightarrow Pb + H_2S \qquad \Delta G^\circ = +177.66\ \text{KJ} \quad (4)$$

$$4Hg^{2+} + 4e \Longleftrightarrow 2Hg + Hg_2^{2+} \qquad \Delta G^\circ = -129.31\ \text{KJ} \quad (5)$$

$$Pb + 2S^{2-} + 4Hg^{2+} + 4e \Longleftrightarrow PbS + HS^- + 2Hg + Hg_2^{2+}$$

$$\Delta G^\circ = -249.81\ \text{KJ}. \quad (6)$$

Based on the Gibbs free energy values obtained from the thermodynamic equilibrium analysis, the Hg^{2+} ionization state is probably present in the volume of PbS under our working conditions. Deposition includes different limiting physical and chemical processes which determine the kinetic behaviour of the doped PbS. (i) *The nucleation stage* is the initial one requiring high activation energy, because the reactive centres (nuclei) are formed on the surface of the substrate. (ii) *The growth stage* is the second one, characterized by an enhanced rate of PbS deposition. (iii) *The doped stage* is the third, where the high rate of deposition is associated to a high level of doping, with the accelerated growth of PbS doped nuclei on the substrate during the nucleation stage. Finally, (iv) *the termination stage* is where the rate of deposition gradually slows down, probably due to a depletion of the reagents.

Preparation of polycrystalline PbS thin films on glass substrates was performed at a temperature of 40 ± 2°C, both undoped and doped with $V_{[Hg^{2+}]}$ grown by chemical bath (CB) and pH = 11.0. The glass substrates were previously immersed in a $K_2Cr_2O_7/HCl/H_2O$ solution for 24 h and then rinsed with deionised water and dried with clean hot-air. PbS films with six different levels of doping $V_{[Hg^{2+}]}$ were obtained by the addition in situ of 5, 10, 15, 20, and 25 mLs in the solutions for PbS growth $Pb(CH_3CO_3)_2$ (0.01 M), KOH (0.5 M), NH_4NO_3 (1.5 M), and $SC(NH_2)_2$ (0.2 M). The solutions were mixed and the final solution kept at 40 ± 2°C during 0.5 h, while the substrate remains inside the solution. The optimal doping concentration $[V_{[Hg^{2+}]}]$ $Hg(NO_3)_2$ (0.031 M) was determined after several trials, when the films had attained good adherence. This solution is routinely added to the reaction mixture during the growth of the PbS films. All the solutions used were prepared with deionised water with a resistivity of 18.2 MΩ. The samples were labelled as PbSHg0 for the undoped sample and $PbSHg_x$ (x = 5, 10, 15, 20, and 25) for the doped samples. The total volume of the growing-solution consisted of the volume-solution (V_{PbS}) for the PbS growth plus the volume-solution $V_{[Ni^{2+}]}$ containing the doping Hg^{2+} chemical agent: $V_{PbS} + V_{[Hg^{2+}]} = V_{tot}$. The films were silver-colored, polycrystalline, and with a homogeneous consistency and good adhesion to the substrate. The substrates were fixed vertically in the chemical bath at correspondance deposition temperature (T_d) for different periods. For first 13 min of reaction time, the solution remained transparent, indicating the occurrence of decomposition reaction. Beyond 15 min, the solution turned dark gray, indicating the formation of PbS nucleus. After completion of the deposition time, samples were removed from the solution, rinsed ultrasonically in hot deionized water for 5 min, and dried in air. Mirror-like gray thin film surfaces were obtained after removal of one side of glass slide using cotton with acid-chromium $K_2Cr_2O_7/HCl/H_2O$ mixture.

3. Results and Discussion

3.1. SEM-EDS. The elemental analysis was performed only for Pb, S, and Hg, while the average atomic percentage

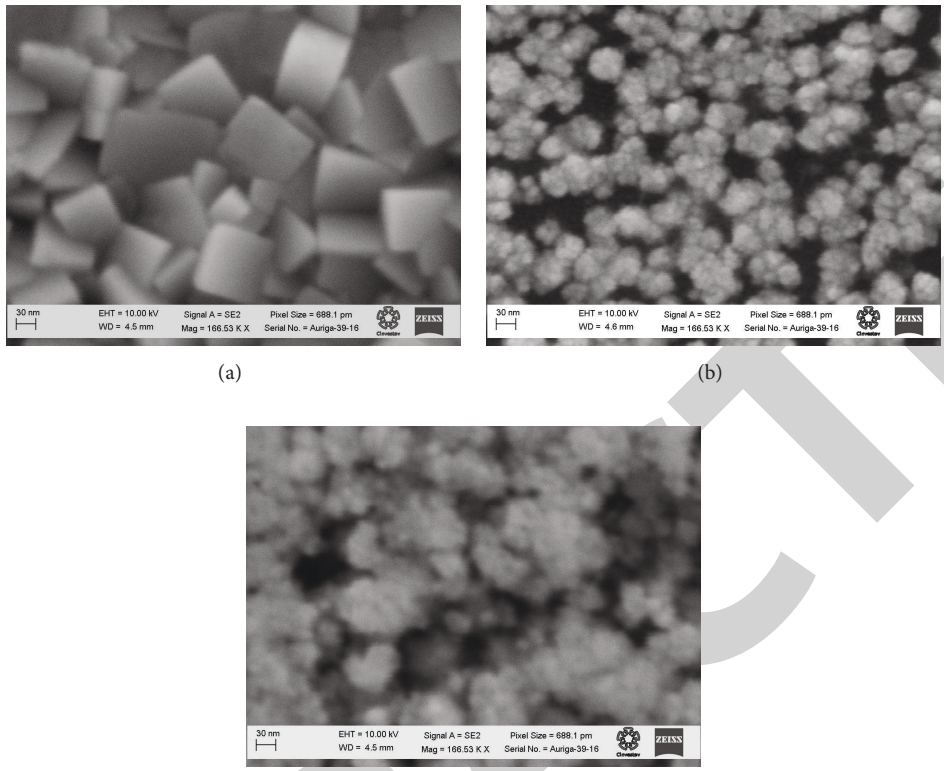

Figure 1: Micrographs of undoped (a) and doped ((b) and (c)) PbS films.

Table 1: The atomic concentrations of Pb, S, and Hg.

Sample	Atomic concentrations		
	Pb	S	Hg
PbS-Hg0	58.35	45.05	0.0
PbS-Hg15	48.10	42.38	9.62
PbS-Hg25	56.29	33.49	10.22

of undoped and doped Pb/S was calculated. The films semiquantitative analysis was carried out by using the EDS technique, for undoped and doped PbS thin films, at different locations, to study their stoichiometry. Table 1 contains the atomic concentrations of Pb, S, and Hg. For the samples, the increase in concentration of Hg in PbS films is easily noted, reaching a percent value of Hg = 11.51. In this case, when Hg^{2+} ion enters as a substitute of the Pb^{2+} ion, it is observed that the sample was slightly deficient in S^{2-} ion. Therefore, for the higher $V_{[Hg^{2+}]}$ values considered here, the material growth can probably be estimated as a doped semiconductor but the material can also be regarded as similar to a solid solution of $Pb_{1-x}H_xS$. It can also be considered how the concentration of Hg in PbS films increases, reaching a percent value of Hg = 11.51. In this case, when the Hg^{2+} ion enters as substitute of the Pb^{2+} ion, probably for the higher $V_{[Hg^{2+}]}$ values considered here the growth material can also be estimated as a doped semiconductor being the material also as in the aforementioned conditions, similar to a solid solution of $Pb_{1-x}Hg_xS$. The micrographs of undoped and doped PbS films are shown in Figure 1 and show scale bars at 30 nm and labeled as: (a) undoped-PbSHg0, (b) doped-PbSHg15, and (c) doped-PbSHg25. As can be seen from the uniform surface morphology, the aspect is compact and of polycrystalline nature. The SEM micrograph shows that the particle grain size decreases as $V_{[Hg^{2+}]}$ concentration increases. The granules appeared to be of different sizes, and it can be concluded that the doping plays a vital role on the morphological properties of the thin PbS films. In such micrographs for the doped films, crystals as small spheres are observed and the degree of crystallinity decreases when increases the concentration of Hg as shown in Figure 2. A very adherent film with metallic gray-black colour aspect was obtained for doped films revealing continuous and compact polycrystalline films. Similar morphologies have been reported [7, 16]. Based on systematic studies of varying $V_{[Hg^{2+}]}$ values, we have discovered the critical factor determining architectural features of PbSHg nanocrystals.

3.2. XRD. Figure 2 shows X-ray diffractograms for doped and undoped films. Such spectra display peaks located at the following angular positions: 2θ = 26.00°, 30.07°, 43.10°, 51.00°, and 53.48°, related to the [111], [200], [220], [311],

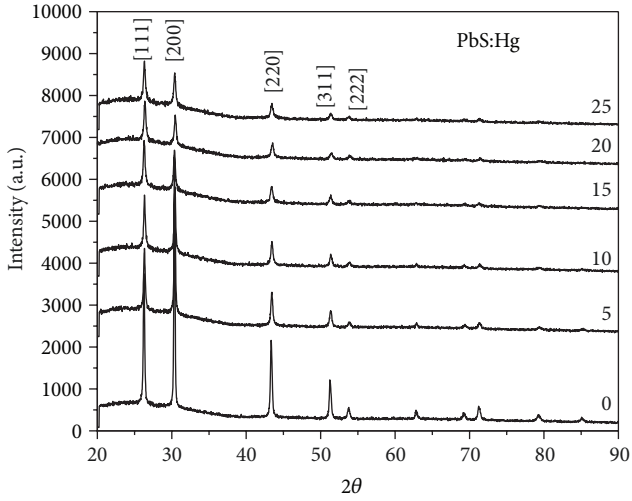

Figure 2: Diffractograms of X-ray (XRD) for doped and undoped PbS films.

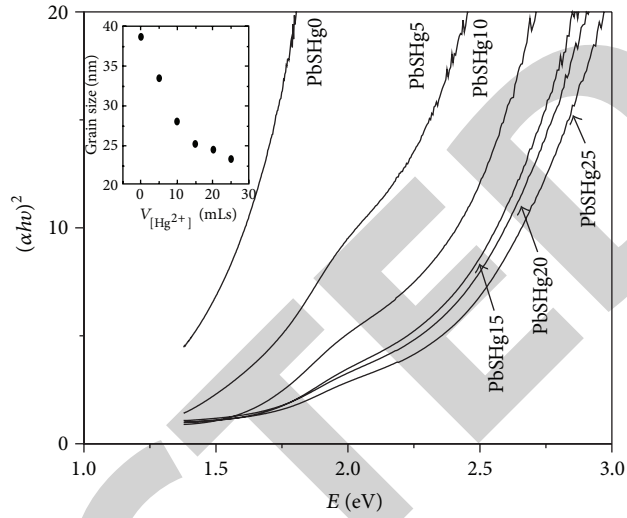

Figure 3: Graph shows $(\alpha h\nu)^2$ versus energy of PbS films. Inset shows average grain size (GS) versus $V_{[Hg^{2+}]}$ for the undoped and doped PbSHg samples corresponding to the [220] plane.

and [222] planes, respectively. These diffraction peaks can be perfectly indexed to diffractograms of the undoped and doped PbS samples displaying the (ZB) crystallinity phase, according to reference patterns JCPDS 05-0592. The XRD spectra for PbSHg0-PbS25 films indicate that [111] is the orientation. The diffraction layer along the [111] plane shows the highest intensity of a well-defined sharp peak, indicating high crystallinity. Using the more intense peak for [111] plane and Bragg's law, the lattice dimension is $a = 5.94$ Å because (ZB) phase belongs to the cubic crystal system. A maximum value in the intensity peak is reached for the prepared sample, indicating either the existence of a larger number of [111] planes or that the [111] planes have a lower number of defects. This phenomenon may be attributed to the doping effect. The low intensity peaks observed in the XRD patterns of the doped PbSHg20 and PbSHg25 samples indicate that the films are coarsely fine crystallites or nanocrystalline. The displayed pattern is due to an amorphous glass substrate and also to some amorphous phase present in the PbSHg crystallite size of films. There are two main possible causes for peak broadening, the increase in heterogeneity of the films due to the occupation of Hg^{2+} into the host lattice and the decrease in crystallite size. These effects are associated with the doped-PbSHg with $V_{[Hg^{2+}]}$ nanocrystals in the regime where the cluster mechanism is dominating, contrary to films grown via ion-ion mechanism, where the crystal size was larger, consisting of PbSHg nanocrystals embedded in an apparent matrix of PbS. A possible explanation is as follows: the ionic radii data are $Pb^{+2} = 1.21$ Å, $S^{2-} = 1.84$ Å, and $Hg^{2+} = 1.10$ Å, and therefore for a relative low concentration of Hg^{2+} ions a majority can be located in (i) Pb^{2+} vacancies sites, which otherwise would be empty (ii) in Pb^{2+} sites causing the appearance of Pb interstitial, and (iii) in interstitial positions. It can be mentioned that the stable crystal structure of PbS, when Hg^{2+} occupies more and more sites of Pb^{2+} in the host lattice, increases internal strain and the crystal structure of PbSHg solid solution becomes unstable. In order to stabilize the crystal structure, the grain size is reduced to release the strain. As the Hg^{2+} concentration is increased, the diffraction peaks become broader due to reduction in the grain size. At this level of $V_{[Hg^{2+}]}$, the PbSHg can be considered as a doped material [6]. The incorporation of Hg^{2+} solubility has been proven to be more effective in Pb chalcogenide than Zn-chalcogenide, a result explained in terms of the cation size.

The inset of the Figure 3 shows the average grain size (GS) versus $V_{[Hg^{2+}]}$ for the undoped and doped PbS samples corresponding to the [220] plane. The GS decreases and GS ~38 nm for PbSHg0. The effect of the GS decrease by the doping effect has been reported in films of PbS doped [6]. A decrease in the degree of order of crystallites is expected to lead to enhanced growth of stable nuclei at the initial stages of growth, followed by impaired grain growth, and, hence resulting in smaller grains of Hg.

3.3. Optical Absorption. Through the intersection of the straight line with the axis of the photon energy, an E_g value is obtained in a similar way to all samples. Figure 3 shows a graph of E_g versus $V_{[Hg^{2+}]}$. In this plot, it can be observed that $E_g = 1.4$ eV for the PbSHg0 sample. The confinement effect appears as a shift in the edge of the absorption spectra and the absorption to lower wavelengths, possibly due to the decrease in GS, the decrease in number of defects, and the change in color. It is clearly seen, from the optical spectrum, an absorption edge shift toward a lower wavelength in doped films. This clearly indicates an increase in the band gap as a result of Hg doping. Doping of PbS with Hg is expected to alter the optical band gap between 0.41 eV, E_g of PbS, in the resulting ternary PbSHg alloy. Thus, the observed large modification of ternary PbSHg alloy shows the existence of strong quantum confinement in this system. The experimentally observed E_g values for the shift indicated an alloying in nanocrystalline PbS. Such increase has been observed [17, 18].

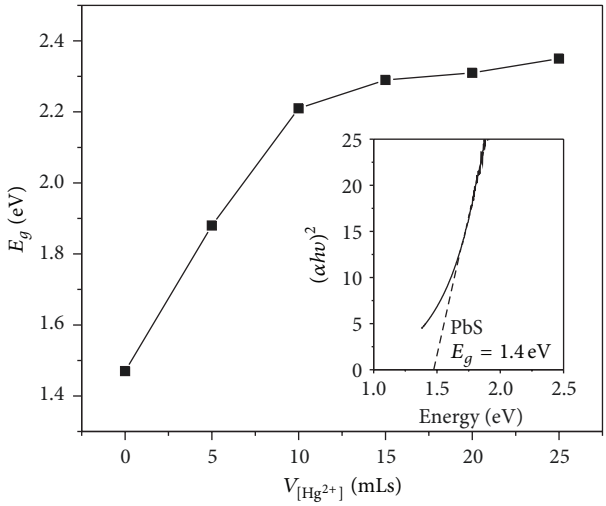

Figure 4: Band gap energy (E_g) as function of $V_{[Hg^{2+}]}$. The inset illustrates the method to calculate E_g from optical absorption measurements.

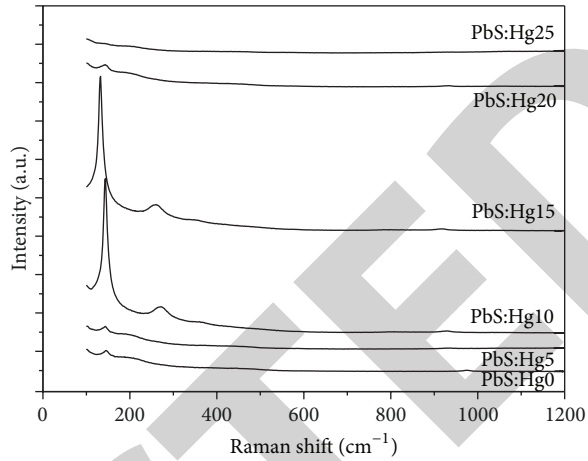

Figure 5: Raman spectra for the films undoped and doped of PbS films.

The E_g for doped samples in the 1.4–2.4 eV range shows the extent of quantum size effect in the nanoparticle films. The fundamental optical transition of doped films (E_g = 0.41 eV) is not observed in these doped films, presumably because of complete mixing of PbS with Hg^{2+} affording a unique ternary intermetallic compound of the $Pb_xHg_{1-x}S$ type [1]. It is observed that the size effect on the optical band gap is stronger in nanoparticle films than in PbS nanoparticle of 24–10 nm (average crystallite size) with E_g from 2.22 to 2.65 eV [2]. The observed increase in the quantum size effect could possibly be attributed to a decrease in the effective mass [19–21]. The increase in E_g with concentration of $V_{[Hg^{2+}]}$ in the films is revealed by the presence of an excitonic structure material. Excitonic structures are readily observed in large E_g semiconductors with binding energy such as CdSe [22]. The E_g optical doped films varied from 1.4 to 2.4 eV, with doping increase of $V_{[Hg^{2+}]}$. A similar shift observed in the position of the excitonic peak towards higher energies in CdSe crystallites has been explained due to a decrease in crystallite size [23]. The redshift of the band gap is associated with the decline of the SG. It is clear that the E_g increases as the $V_{[Hg^{2+}]}$ increases. As mentioned earlier, we observed a systematic decrease in the crystallite size with increasing concentration. Since the estimated mean crystallite size in this case is approximately half the value of the exciton Bohr radius in PbS, we observe a strong confinement in doped PbSHg films. Using published data, a nanocrystalline size of 4-5 nm corresponding to E_g = 1–1.25 eV, 3.8 nm for E_g = 1.4 eV, 2.7 nm for E_g = 2.0 eV, and 2 nm for E_g = 2.7–3.8 eV, respectively, was calculated [19].

Figure 4 shows a plot of E_g versus $V_{[Hg^{2+}]}$ and the absorption spectrum of PbSHg0 is in the lower part. In our case, the introduction of Hg^{2+} ions into PbS induced the increase of strain. On the other hand, the creations of S^{2-} vacancies relax the lattice. Strain in PbSHg tends to redsuce GS. When doping, the number of the nucleation centers increases both in the substrates and in the solution, and, in this way, the nucleation rate becomes larger than the growth rate leading to a broader dispersion in GS and to a decrease of this one.

3.4. Raman. The 514.5 nm wavelength laser Raman spectroscopy was used to analyze the films. The spectra displayed undoped and doped PbS films in Figure 5 show the same wavenumbers at 135, 217, 433, and 647 cm^{-1}. Peaks corresponded to the fundamental longitudinal optical (LO) phonon mode of rock-salt structure, first overtone (2LO), and second overtone (3LO), respectively. The strong band in ~133–140 cm^{-1} is attributed to a combination of longitudinal and transversal acoustic modes [24]. It has been reported that the band centred at 961 cm^{-1} could be due to sulphates in the sample not the laser-induced degradation [24, 25], which is consistent with the results reported [26]. However, in our samples, the XRD patterns of PbS undoped and doped structures confirm that the product consists of PbS pure cubic without the presence of sulphates. It should be noted that data from PbS nanoparticles (18 nm in diameter) in air at room temperature have shown the LO band to be at ~210 cm^{-1} with a small shoulder, attributed to an SP mode at 205 cm^{-1}; however, a downward trend in wave number was shown for the former as the size of particles was increased to 38 nm diameter [26].

4. Conclusions

We have reported the growth of doped PbS with Hg^{2+} ions affording nanocrystalline films by the chemical bath technique. X-ray spectra show 2θ = 26.00°, 30.07°, 43.10°, 51.00°, and 53.48°, which belong to the ZB phase. The grain size ranges from ~32 to 20 nm. Optical absorption spectra are quantified for the PbSHg film in which the redshift of band gap is associated with the decrease of the average GS. Forbidden band gap energy E_g shifts in the range 1.4–2.4 eV. Raman spectroscopy (RS) exhibited an absorption band ~135 cm^{-1} displaying only a PbS ZB structure.

Acknowledgments

The authors thank Lic. Damián Hernández Méndez, Principal of AGU, and C.P. Laura Rojas of VD of Benemérita Universidad Autónoma de Puebla.

References

[1] A. P. Gaiduk, P. I. Gaiduk, and A. N. Larsen, "Chemical bath deposition of PbS nanocrystals: effect of substrate," *Thin Solid Films*, vol. 516, no. 12, pp. 3791–3795, 2008.

[2] R. K. Joshi, A. Kanjilal, and H. K. Sehgal, "Size dependence of optical properties in solution-grown $Pb_{1-x}Fe_xS$ nanoparticle films," *Nanotechnology*, vol. 14, no. 7, pp. 809–812, 2003.

[3] Y. F. Nicolau, M. Dupuy, and M. Brunel, "ZnS, CdS, and $Zn_{1-x}Cd_xS$ thin films deposited by the successive ionic layer adsorption and reaction process," *Journal of the Electrochemical Society*, vol. 137, no. 9, pp. 2915–2924, 1990.

[4] S. C. Ray, M. K. Karanjai, and M. K. D, "Deposition and characterization of $Zn_xCd_{1-x}S$ thin films prepared by the dip technique," *Dashupta Thin Solid Films*, vol. 332, pp. 117–122, 1998.

[5] L. P. Deshmukh, K. M. Garadkar, and D. S. Sutrave, "Studies on solution grown $Hg_xCd_{1-x}S$ thin films," *Materials Chemistry and Physics*, vol. 55, no. 1, pp. 30–35, 1998.

[6] O. Portillo-Moreno, H. Lima-Lima, V. Ramírez-Falcon et al., "Growth of CdS:Cu nanocrystals by chemical synthesis," *Journal of the Electrochemical Society*, vol. 153, no. 10, pp. G926–G930, 2006.

[7] O. Portillo Moreno, L. A. Chaltel Lima, M. Chávez Portillo et al., "Properties of PbS: Ni^{2+} nanocrystals in thin films by chemical bath deposition," *ISRN Nanotechnology*, vol. 2012, Article ID 546027, 12 pages, 2012.

[8] K. P. Acharya, N. N. Hewa-Kasakarage, T. R. Alabi et al., "Synthesis of PbS/TiO_2 colloidal heterostructures for photovoltaic applications," *Journal of Physical Chemistry C*, vol. 114, no. 29, pp. 12496–12504, 2010.

[9] J. B. Biswal, N. V. Sawant, and S. S. Garje, "Deposition of rod-shaped antimony sulfide thin films from single-source antimony thiosemicarbazone precursors," *Thin Solid Films*, vol. 518, no. 12, pp. 3164–3168, 2010.

[10] K. Rakesh, A. K. Joshi, and H. K. Shegal, "Solution grown PbS nanoparticle films," *Applied Surface Science*, vol. 221, pp. 43–47, 2004.

[11] S. Thangavel, S. Ganesan, S. Chandramohan, P. Sudhagar, Y. S. Kang, and C.-H. Hong, "Band gap engineering in PbS nanostructured thin films from near-infrared down to visible range by in situ Cd-doping," *Journal of Alloys and Compounds*, vol. 495, no. 1, pp. 234–237, 2010.

[12] M. Wanili, J. M. Luther, H. Zheng, Y. Wu, and P. Alivisatos, "Photovoltaic devices employing ternary PbS_xSe_{1-x} nanocrystals," *Nanoletters*, vol. 9, pp. 1699–1703, 2009.

[13] S. Wu, H. Zeng, and Z. A. Schelly, "Preparation of ultrasmall, uncapped PbS quantum dots via electroporation of vesicles," *Langmuir*, vol. 21, no. 2, pp. 686–691, 2005.

[14] J. Xu, D. Cui, T. Zhu et al., "Synthesis and surface modification of PbSe/PbS core-shell nanocrystals for potential device applications," *Nanotechnology*, vol. 17, no. 21, pp. 5428–5434, 2006.

[15] O. Portillo-Moreno, H. Lima-Lima, R. Lozada-Morales, R. Palomino-Merino, and O. Zelaya-Angel, "$Cd(S_{(1-x)} + CO_{3(x)})$ thin films by chemical synthesis," *Journal of Materials Science*, vol. 40, no. 17, pp. 4489–4492, 2005.

[16] E. Pentia, L. Pintillie, T. Matei, and B. E. Ozbay, "Chemically prepared nanocrystalline PbS thin films," *Journal of Optoelectronics and Advanced Materials*, vol. 3, no. 2, pp. 525–530, 2001.

[17] R. Kostic, M. Romcevic, N. Romcevic et al., "Photoluminescence and far-infrared spectroscopy of PbS quantum dots—polyvinyl alcohol nanocomposite," *Optical Materials*, vol. 30, pp. 1177–1182, 2010.

[18] U. Lunz, J. Kuhn, F. Goschenhofer et al., "Temperature dependence of the energy gap of zinc-blende CdSe and $Cd_{1-x}Zn_xSe$ epitaxial layers," *Journal of Applied Physics*, vol. 80, no. 12, pp. 6861–6863, 1996.

[19] O. Portillo Moreno, R. Lozada Morales, M. Rubín-Falfán, J. A. Pérez-Álvarez, O. Zelaya-Angel, and L. Baños-López, "Phase transformation on CdSe thin films under annealing in $Ar+Se_2$ atmosphere," *Journal of Physics and Chemistry of Solids*, vol. 61, pp. 1751–1754, 2000.

[20] A. Popa, M. Lisca, V. Stancu, M. Buda, E. Pentia, and T. Botila, "Crystallite size effect in PbS thin films grown on glass substrates by chemical bath deposition," *Journal of Optoelectronics and Advanced Materials*, vol. 8, no. 1, pp. 43–45, 2006.

[21] B. K. Rai, H. D. Bist, R. S. Katiyar, M. T. S. Nair, P. K. Nair, and A. Mannivannan, "Simultaneous observation of strong and weak quantum confinement effect in chemically deposited CdSe thin films: a spectro-structural study," *Journal of Applied Physics*, vol. 82, no. 3, pp. 1310–1319, 1997.

[22] I. Balberg, E. Savir, Y. Dover, O. P. Moreno, R. Lozada-Morales, and O. Zelaya-Angel, "Meyer-Neldel-like manifestation of the quantum confinement effect in solid ensembles of semiconductor quantum dots," *Physical Review B*, vol. 75, no. 15, Article ID 153301, 4 pages, 2007.

[23] A. Rivera Márquez, M. Rubín Falfán, R. Lozada Morales et al., "Quantum confinement and crystalline structure of CdSe nanocrystalline films," *Physics of the Solid State*, vol. 188, no. 3, pp. 1059–1064, 2001.

[24] A. Phuruangrat, T. Thongtem, and S. Thongtem, "Characterization and photoluminescence of pbs nanocubes synthesized by a solvothermal method," *Chalcogenide Letters*, vol. 8, no. 5, pp. 297–300, 2011.

[25] G. D. Smith, S. Firth, R. J. H. Clark, and M. Cardona, "First- and second-order Raman spectra of galena (PbS)," *Journal of Applied Physics*, vol. 92, no. 8, pp. 4375–4381, 2002.

[26] S. Xiong, B. Xi, D. Xu et al., "L-cysteine-assisted tunable synthesis of PbS of various morphologies," *Journal of Physical Chemistry C*, vol. 111, no. 45, pp. 16761–16767, 2007.